

EFFECT OF DAMAGE ON ELECTROMAGNETIC SHIELDING PROPERTIES OF CARBON FIBRE REINFORCED COMPOSITES

E. Mikinka¹, G. Zhou¹, T. Whittaker², W. Whittow² and W. Sun³

¹ Department of Aeronautical and Automotive Engineering, Loughborough University, Loughborough, United Kingdom, e.e.mikinka@lboro.ac.uk, lboro.ac.uk/departments/aae/

² Wolfson School of MEME, Loughborough University, Loughborough, United Kingdom, t.whittaker@lboro.ac.uk, lboro.ac.uk/departments/meme/

³ C-Power Ltd, Tianjing, China, zhonglizhidian@cpower.com.cn

Keywords: Composite laminates, Carbon fibres, Electromagnetic shielding, Impact damage

ABSTRACT

The overwhelming majority of studies concerning impact damage in carbon fibre/epoxy composites have so far been conducted in the context of the damage tolerance with little attention paid to the effect on other properties. Electromagnetic shielding is one of the emerging application areas of carbon fibre reinforced composites, which, due to the good electrical conductivity, high specific strength and resistance to corrosion, constitute an attractive alternative to traditionally used metal alloys. This paper presents the results of a preliminary study on the electromagnetic shielding durability of multilayer carbon epoxy composites in four different configurations. The laminates were first subjected to a low-velocity impact and scanned for damage area using non-destructive ultrasonic and infrared thermography methods. The shielding effectiveness (SE) of the damaged specimens was then measured in the low frequency range using coaxial transmission line and in the high frequency range using free-space transmission method. Comparison of the transmission responses for pristine and impacted composites showed that at low frequencies the SE increased slightly due to delamination damage, which created additional interfaces to interact with the electromagnetic wave. These additional internal reflection coefficients increased the absorption capabilities of the composite without affecting the reflection losses, as confirmed by the shielding mode analysis. When the impact energy was increased causing impactor penetration, both the reflection and absorption loss of the composite were reduced due to the interruptions in the conductive network. No changes in the SE due to the impact damage were observed in the high frequency range for any of the investigated composite configurations, which was attributed to the reduced skin depth disabling significant EM wave fraction from reaching the delaminated region in combination with the limited dynamic range of the measuring equipment.

1 INTRODUCTION

The combination of high specific strength, stiffness and corrosion resistance makes carbon fibre reinforced polymer (CFRP) composites an attractive replacement of metals not only in primary load-bearing structures but also in the electrical engineering sector, owing to their good electrical conductivity. Examples include CFRPs implemented as waveguides [1] or antenna structures [2] as well as ground planes in monopole antennas [3]. Over recent years, it has been demonstrated that CFRP composites can be a promising candidate for electromagnetic (EM) shielding structures [4-6], combining mechanical and electrical properties with design versatility. Electromagnetic interference (EMI) is becoming a serious problem nowadays as the number of electronic devices emitting EM radiation is rapidly increasing. Moreover, modern electronic devices are densely integrated and operate at relatively low voltages, which makes them particularly vulnerable to the perturbation caused by the EMI. Implementation of a shielding structure is the simplest way to address the problem of EMI.

Unlike monolithic metal alloys, CFRP composite materials are vulnerable to the impact damage due to the lack of through-the-thickness reinforcement and brittle nature of carbon fibres. As a result,

an impairment in the mechanical properties, in particular compressive strength, in the aftermath of the impact event is commonly observed. So far, although both the shielding properties and impact damage resistance of CFRP composites have been thoroughly characterised in a large number of studies, the EM shielding durability, i.e. the ability to maintain electromagnetic shielding properties after sustaining a mechanical damage, has not been examined at all; the only reported work concerns non-structural self-healing materials [7-8]. This paper reports on an experimental investigation into the effect of the low-velocity impact damage on the EM shielding properties of CFRP composites with different thicknesses and lay-ups evaluated in both low and high frequency regimes. A parametric study concerning a range of impact energies and composite configurations is implemented to get a deeper insight into the factors directly influencing the electromagnetic shielding durability. As a desired outcome, the scientific base for the eventual realization of a coherent set of design principle for damage-tolerant EM shielding composites will be built-up, allowing for a more efficient design of non-metallic EM shielding structures.

2 ELECTROMAGNETIC SHIELDING THEORY

In most general terms, the EM shielding effectiveness (SE) is expressed in decibels and defined as a ratio of the incident to transmitted electric (or magnetic) power or field by the relationship:

$$SE=10*\log(P_i/P_t)=20*\log(E_i/E_t)= 20*\log(H_i/H_t). \quad (1)$$

where P , E and H correspond to the EM power, electric and magnetic field, respectively and subscripts i and t indicate incident and transmitted quantities.

The basic EM shielding theory corresponds to shielding of an EM plane wave in the far field, where the wave impedance in free space (ratio of the transverse components of the electric and magnetic fields) is constant and independent of the distance from the source so that the SE is only a function of material properties and incident radiation frequency. For thin and conducting materials, the equations have been derived based on the transmission line theory by Schelkunoff [9], where three contributions to the total SE are distinguished, namely reflection (SE_R), absorption (SE_A) and multiple reflections. The reflection loss is related the impedance mismatch between the free space and material, whereas the absorption loss is a result of interaction of EM wave photons with the electric and magnetic dipoles in the material. Multiple reflections might occur if the material has many interfaces with varying impedances. It is generally assumed that this mechanism is negligible if the absorption loss exceeds 15dB or the thickness is larger than the skin depth. The reflection and absorption losses can be derived as a function of radiation frequency ν , material thickness t and intrinsic properties of the material such as electrical conductivity σ and magnetic permeability μ :

$$SE_R=168-10*\log(\nu\mu/\sigma), \quad (2)$$

$$SE_A=3.34*t*(\nu\mu\sigma)^{1/2}. \quad (3)$$

3 EXPERIMENTAL DETAILS

3.1 Composite manufacturing and test sample preparation

Carbon fibre reinforced composites investigated in this study were manufactured from unidirectional (UD) LTM45/34-700 prepreg tape with a nominal ply thickness of 0.125mm. Individual 300x300 mm plies were cut from the prepreg roll and laid up in a lay-up of cross-ply ($[0^\circ/90^\circ]_{ns}$) and quasi isotropic ($[45^\circ/0^\circ/-45^\circ/90^\circ]_{ns}$). The stacks with eight and sixteen plies were cured in the autoclave at 60°C under the pressure of 0.62 MPa for 16 hours. Thin 8-ply and thick 16-ply composites had thicknesses of 1 and 2 mm respectively. The cured laminates were cut into square 150x150 mm samples using Bella Maxitile 260 water-cooled bench saw. Circular samples for low-frequency SE characterisation were cut from the square specimens after impact testing using CNC machine.

3.2 Low-velocity impact tests

All impact tests were conducted using a purpose-built guided drop-weight impact rig with a 1.5 kg strain-gauged impactor having a 20mm diameter hemispherical nose. The initial impact velocity was measured using T1000 high precision laser trigger connected to the C3008 data acquisition system provided by Imatek Systems. Force-time history was recorded for each impact. Impact energies ranging from 8 to 25J were varied as shown in Table 1 by adjusting the drop height. For samples to be tested for SE in the high frequency range the impact was in the centre, however, the impact location was off-centre to coincide with the illuminated region in the coaxial transmission line. All impacted specimens were non-destructively tested using ultrasonic pulse echo scanner (Dolphicam2) and infrared thermography (EchoTherm system) to obtain accurate information on the shape and size of the delamination.

Sample Number	Impact energies for low frequency SE test samples (J)	Impact energy for high frequency SE test samples (J)
8-ply CP	8	11, 12
8-ply QI	8, 15	10, 12
16-ply CP	15	22, 25
16-ply QI	12	20, 25

Table 1: Impact test energies for carbon/epoxy laminates tested in this study.

3.3 Low-frequency SE measurement

All low-frequency shielding measurements were completed by means of a coaxial transmission line method according to the ASTM D4935 standard for measuring SE of planar materials [10]. Its main advantage over other methods is the ability to obtain individual contributions of reflection and absorption modes of shielding. The experimental set-up operating in the frequency range from 30 MHz to 1.5 GHz consisted of a flanged brass coaxial holder connected to the two ports of Rohde & Schwarz ZNLE3 vector network analyzer (VNA) with the lossless UFA210B cables and N-type connectors. The elements of the holder were in-house manufactured and assembled at Loughborough University. To remove the effect of cables and connectors from the results, the VNA was calibrated using ZN-Z170 calibration kit according to the transmission-open-short-match (TOSM) procedure. The schematic diagram of the assembled set-up is shown in Fig. 1. The test procedure, according to the [10], consisted of two separate measurements for each sample type. The first measurement of a reference specimen was performed to repeat the capacitive coupling of the 'load' specimen and thus establish the effect of the discontinuity in the transmission line caused by the sample insertion. When the load sample replaced the reference, the second measurement was carried out and the difference between the two gave the value of the specific S-parameter according to:

$$|S_{ij}|_{dB} = |S_{ij}^{load}|_{dB} - |S_{ij}^{reference}|_{dB} . \quad (4)$$

Recording the full set of complex S-parameters (S_{11} , S_{12} , S_{21} , S_{22}) allowed to calculate the quantities of the absorption (SE_A) and reflection (SE_R) loss, according to Eq. (5-6), where T , R and A corresponded respectively to the transmission, reflection, and absorption coefficient.

$$SE_R = -10 \cdot \log(1-R) = -10 \cdot \log(1-|S_{11}|^2), \quad (5)$$

$$SE_A = -10 \cdot \log(A) = -10 \cdot \log(T/(1-R)) = -10 \cdot \log(|S_{21}|^2 / (1-|S_{11}|^2)), \quad (6)$$

$$SE = -10 \cdot \log(T) = -10 \cdot \log|S_{21}|^2. \quad (7)$$

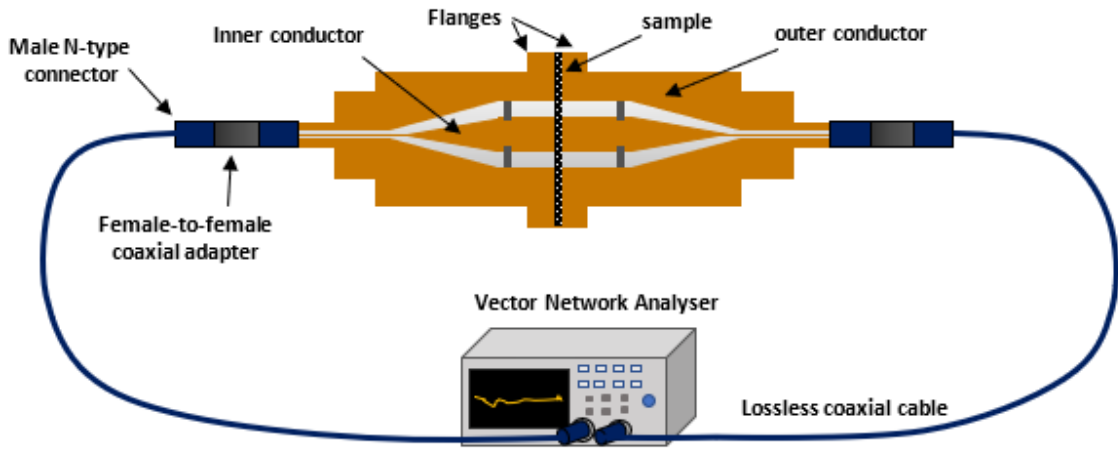


Figure 1: Coaxial transmission line for low frequency SE measurement.

3.4 High-frequency SE measurement

Due to the difficulties in applying transmission line method at higher frequencies, an alternative free-space method was employed in accordance with the recommendations in [11]. The tested specimens were mounted over a square 130mm aperture in a copper plate placed between two Flann22240 horn antennas connected to the ports of Anritsu MS46522B VNA operating in the frequency range from 26 to 42 GHz. 3D printed high impact polystyrene ($\epsilon_r=2.45$) focusing lenses with the diameter of 100mm and focal length of 131.6mm were placed between the test specimen and each antenna as shown in Fig. 2 to avoid diffraction effects at the edges of the sample while keeping the sample size to minimum. In this way it was possible to avoid using a costly anechoic chamber commonly employed in free-space measurement. The set-up was designed according to the Gaussian quasi-optical beam theory based on the assumption that the far field main lobe of a pyramidal horn antenna can be represented as a Gaussian source. The tested specimen was placed at the focal plane, i.e. the distance between the antenna and lens and wells as lens and sample was equal to the focal length. This is because the phase taper is minimised on the focal plane, so that the radius of curvature of the wave fronts is infinite and the fields can thus be approximated as a plane wave. In addition, in this arrangement the output beam radius is independent of the distance between the antenna and the lens. The SE was obtained as a difference in the transmission parameter S_{21} with and without the sample mounted on the copper plate:

$$SE = 20 \cdot \log |S_{21_no_sample}| - 20 \cdot \log |S_{21_sample}|, \quad (8)$$

The set-up was calibrated using the four-parameter method and time-domain gating (built-in feature of VNA) was applied to separate the specimen-related reflection components from other discontinuities within the measurement system.

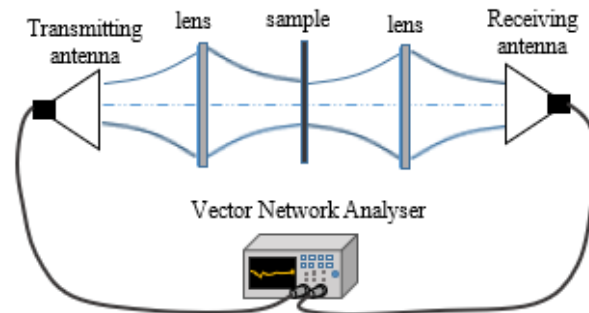


Figure 2: Free-space set-up for high frequency SE measurement.

4 RESULTS AND DISCUSSION

4.1 Low-velocity impact damage in composite samples

The recorded load histories yielded important information regarding the characteristics of damage, including its initiation and growth. In majority of the cases, for the chosen impact energies, the load-time responses had a shape of a primary Gaussian pulse, see Fig. 3a. The changes of the slope in the rising portion of the curve as indicated in Fig. 3b, are attributed to the initialisation of the delamination failure. The elastic impact characteristics disappeared at 12J for the 8-ply quasi-isotropic laminates. The corresponding response was characterised by a sharp load drop after reaching peak load which was followed by an extended region of pronounced force oscillations in the unloading part of the curve. For thick 16-ply laminates similar distinctive behaviour in the unloading portion of the impact response was observed at the highest impact energy of 25J, which in further analysis was ascribed to the extensive back-fibre splitting with the onset of fibre fracture.

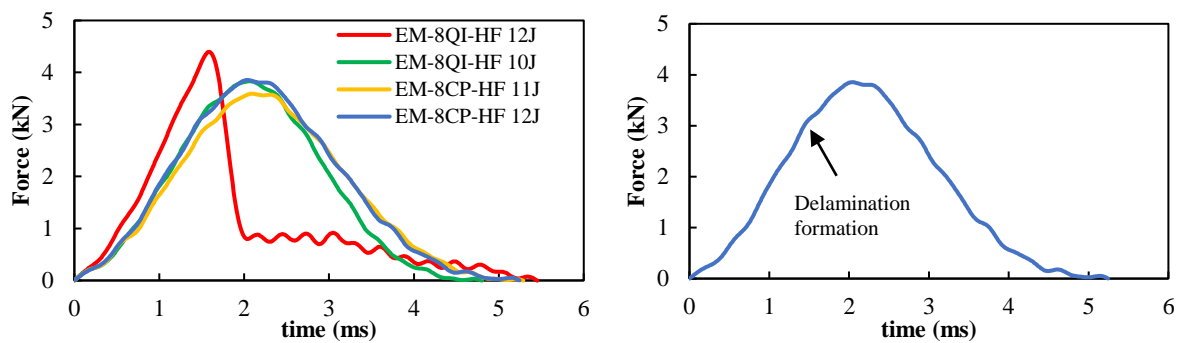


Figure 3: Response curves for a) 8-ply laminates subjected to 10-12J energy impact b) changes in the slope indicating delamination damage in 8-ply CP laminate under 12J impact.

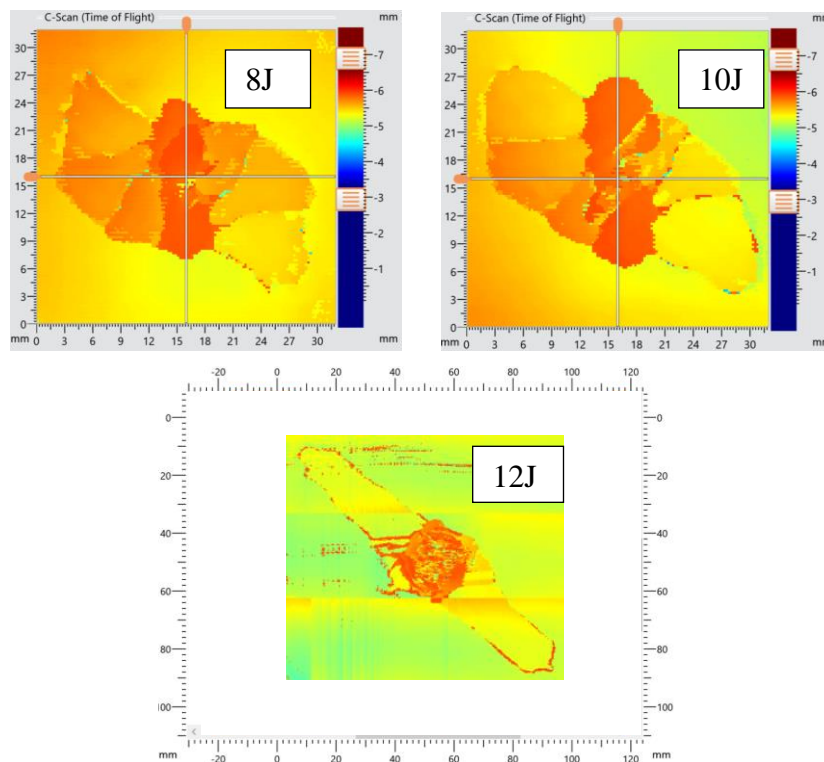


Figure 4: Evolution of damage area with increasing impact energy for 8-QI laminate.

The information obtained from the load histories was further supported by the ultrasonic C-scans and infrared thermograms. For the thin samples to be examined for low-frequency SE and impacted with 8J energy it was confirmed that the delamination area entirely fitted the annular region exposed to the EM radiation. Both the size and shape of the delamination were changing with the increasing impact energy as shown in Fig. 4. The extensive bending stresses in the bottom side of the laminate were responsible for the damage growth along the fibre direction of the bottommost ply at 12J for the 8-ply quasi-isotropic laminate. Little difference in the damage area between 8 and 10J impact energies is most likely associated with the fact that the 8J impact was not-exactly at the laminate centre, which is known to induce stiffer response. With almost doubled impact energy, the same laminate was penetrated by the impactor. The resulting damage modes included extensive push-out delamination with a large amount of fibre breakage and debonding. Ultrasonic C-scanning was not performed and the laminate was only examined using IR thermography as shown in Fig. 5. Finally, for a similar impact energy to thickness ratio, in thicker laminates the damage was found to spread over larger area, which was associated with their higher stiffness causing larger interlaminar stresses.

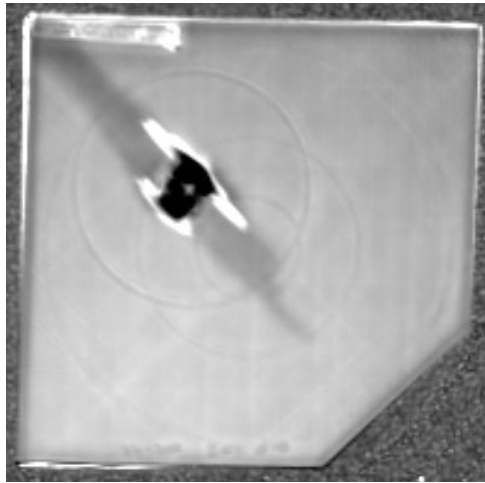


Figure 5: IR thermogram of 8-ply QI laminate subjected to 15J impact damage.

4.2 Shielding effectiveness of pristine carbon/epoxy composites

Using the recorded S-parameters, the corresponding values for the specific modes and total shielding were calculated and plotted as a function of frequency for all four considered composite configurations. The plots are shown in Fig. 6. The SE of all considered composites exhibited very similar frequency dependence, with an initial steady increase followed by a region of constant SE. Within the same thickness, cross-ply and quasi-isotropic composites were found to be equally effective in preventing EM penetration. This is most likely related to the multi-directional orientation of carbon fibres in both cases which coincided with the electric field lines of the coaxial transmission line. While keeping the lay-up identical, thicker laminates were also found to have the SE approximately 10dB higher compared to thin laminates. The SE frequency responses of the thicker laminates were also characterised by more pronounced ripples. The main reason for that behaviour can be linked to the larger number of intra-ply reflections and transmissions as a result of increased number of interfaces.

Fig 7a shows individual contributions to the total SE for the 8-ply quasi-isotropic laminate. The absorption was found to be the dominant shielding mode and its frequency dependence closely resembled that of the total SE. On the other hand, the reflection loss, after initial rise, remained constant and its value did not exceed 18dB. Both reflection and absorption modes of shielding were insensitive to the lay-up, but absorption was found to be affected by the thickness. This confirms that the higher SE observed in thicker laminates was correlated with the higher absorption loss. A shielding profile for both 8- and 16-ply laminates is compared in Fig. 7b.

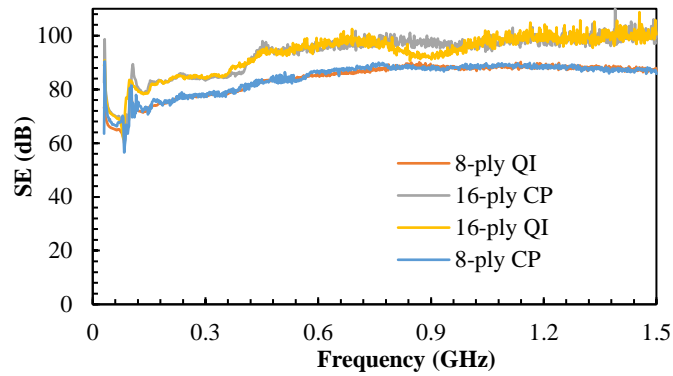


Figure 6: Low-frequency SE of pristine CFRP laminates in all investigated configurations.

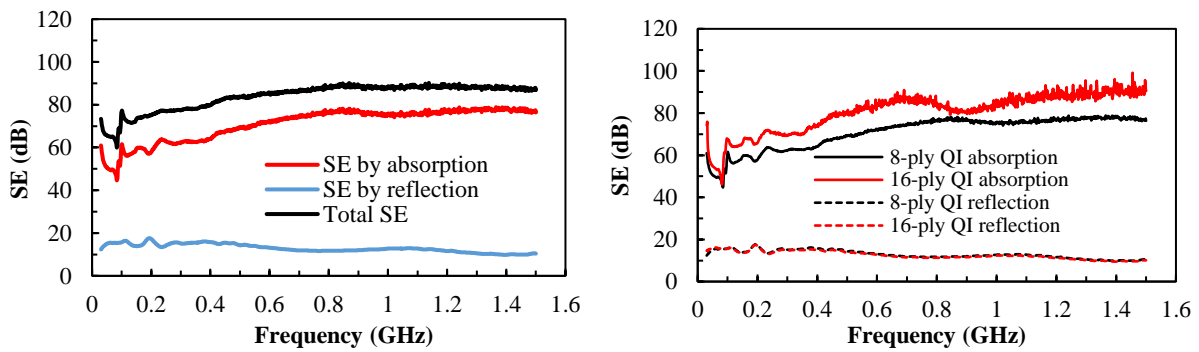


Figure 7: Shielding modes for a) 8-ply QI laminate b) 8- and 16-ply QI laminates.

In the high frequency region between 26 and 42 GHz all four laminates exhibited similar SE. No effects of the thickness or lay-up were observed and the spectra, see Fig. 8, were characterized by multiple peaks. Their presence was associated with the highly reflective nature of carbon fibres and the way in which the free-space set-up was constructed, with the two antennas partitioned by a highly conductive sample. It must be remembered that the absorption is directly proportional to the frequency and even very thin 1 mm laminates provide enormous EM attenuation, which might exceed the dynamic range of the VNA used for the measurements in particular when any of the layers is oriented parallel to the electric field lines. This was the case for all laminate configurations considered in this study. The differences could only be observed for less-reflective composite arrangements with no carbon fibres oriented at 90°.

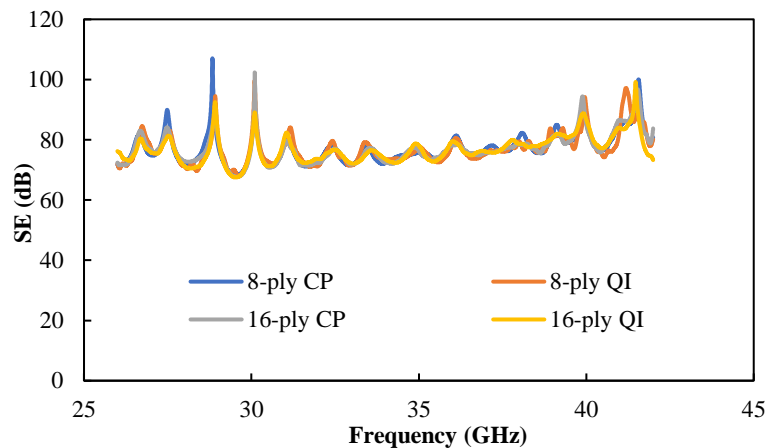


Figure 8: High frequency SE for pristine CFRP laminates.

4.3 Effect of impact damage on shielding effectiveness at low frequencies

By overlaying SE frequency responses of both pristine and impact-damaged composites, the effect of damage on the shielding properties could be assessed. An example of such a plot for a 16-ply CP laminate is shown in Fig. 9. It is observed that although the general trend of the curve remained identical for both the pristine and damaged specimens, the damaged sample was characterized by much more pronounced ripples, whose size increased with the frequency. Extraction of the individual modes contributions, see Fig. 10, implies that the observed SE changes were related to the altered absorption behaviour, with the reflection remaining unaffected. It can be inferred that the delaminations created during the impact event constituted additional interfaces in the laminate, which interacted with the EM wave and slightly enhanced its absorption capabilities. With the outer faces not affected in any significant way for a barely visible impact damage (BVID), the reflection loss, which is determined by the impedance mismatch between air and the material surface, was not changed. Summary of the average SE before and after impact for all considered composite configurations is given in Table 2.

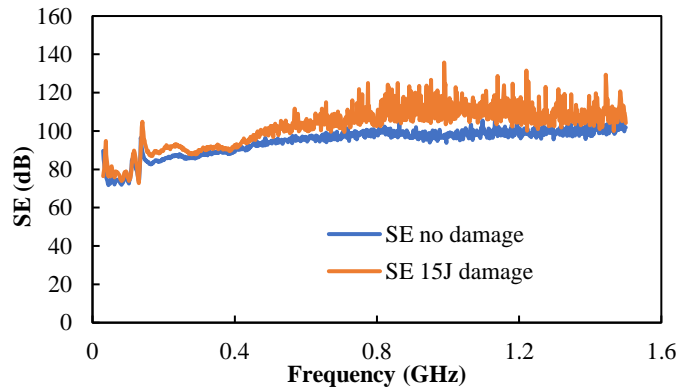


Figure 9: Shielding effectiveness for pristine and damaged 16-ply cross-ply laminate.

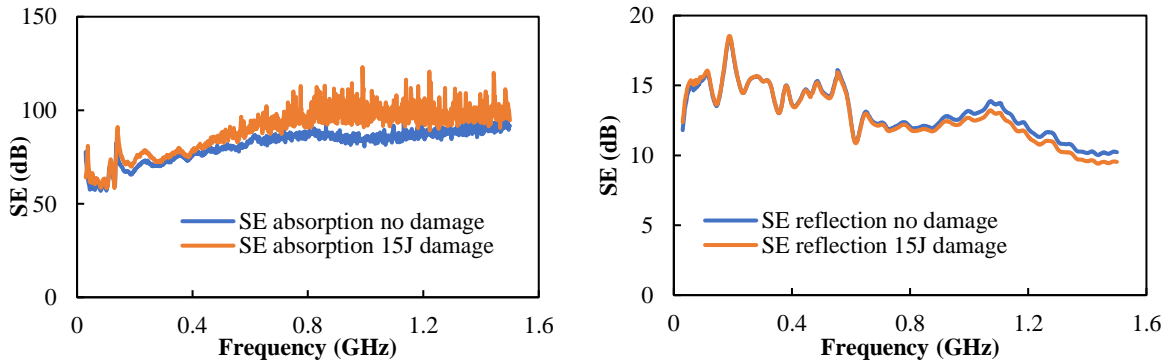


Figure 10: Shielding modes for pristine and damaged 16-ply cross-ply laminate.

Composite lay-up	Impact energy (J)	Average SE before damage (dB)	Average SE after damage (dB)
8CP	8	84.1	85.6
8QI	8	84.0	85.4
8QI	15	84.0	78.0
16CP	15	94.4	103.0
16QI	12	94.9	100.0

Table 2: Summary of the effect of impact damage on average SE.

Increasing the impact energy beyond the BVID limit induced further changes in the SE characteristics. With the energy almost doubled (15J), the 8-ply QI sample was penetrated by the impactor so that the continuity of the carbon fibres was compromised. In consequence, not only absorption but also reflection loss was altered. The interruption of the conductive network caused by carbon fibre fracture reduced the effective reflection cross-section and allowed for an increased penetration and leakage of the electromagnetic wave, which translated into the reduced SE as shown in Fig. 11. Although intuitively the SE should decrease with frequency for the penetrated laminate (as the wavelengths approaches the size of the discontinuity), the SE despite general reduction compared to the baseline, did not exhibit a decreasing trend. This behaviour can be ascribed to the presence of the two competing phenomena, one related to the aperture due to the fractured fibres and another to the increased thickness due to the pushout delamination. As opposed to a ‘clean’ cut-out hole, the opening caused by the impactor is not regular and obscured with multiple fractured protruding fibres, which constitute additional elements capable of attenuating the EM wave. In consequence, the shielding capabilities of the carbon/epoxy composites, in particular in the low-frequency range, could be maintained even after sustaining very severe structural damage.

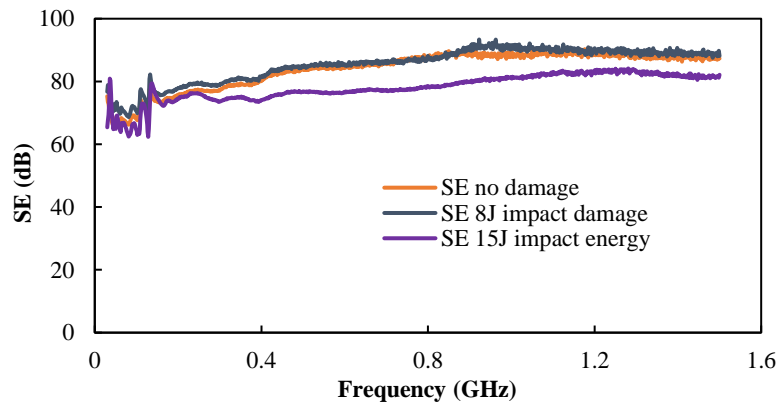


Figure 11: Effect of impact energy on low-frequency SE of 8-ply quasi-isotropic laminate.

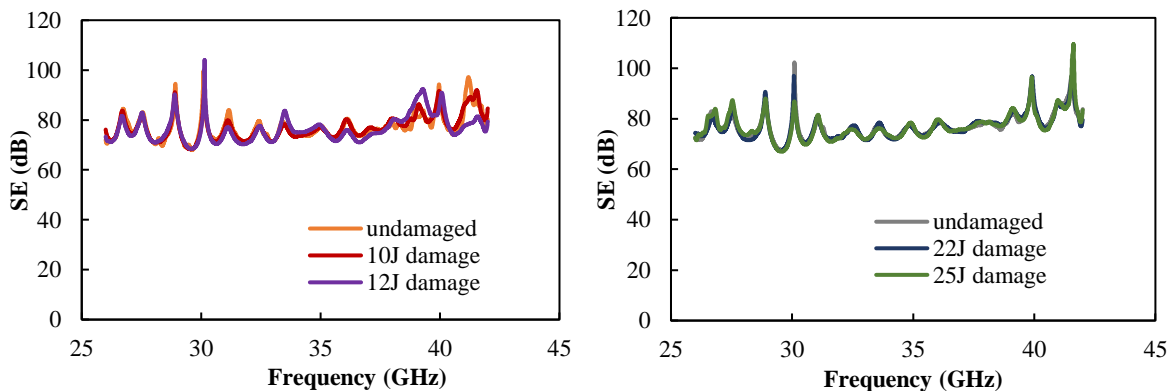


Figure 12: High frequency SE of pristine and damaged 8-ply quasi-isotropic and 16-ply cross-ply laminates.

4.4 Effect of impact damage on shielding effectiveness at high frequencies

Pristine and damaged laminates exhibited almost identical shielding behaviour in the high frequency regime. For all four considered composite configurations, both the magnitude and frequency dependence of SE remained unchanged, regardless of the impact energy level. Fig. 12 shows examples of high frequency SE spectra for the 8-ply quasi-isotropic and 16-ply cross-ply composites before and

after sustaining impact damage at two different energy levels. The fact that no changes in the SE were observed is attributed partially to the damage characteristics, which, for the chosen levels of impact energy, was restricted to delamination without affecting the continuity of the fibres. As a result, the shielding capabilities were not compromised. Although the delamination might have caused some slight improvements in the shielding characteristics as observed in the low-frequency region, the significantly reduced skin depth in the high frequency region and increased absorption losses in the fibres meant that most of the EM wave could not reach the delaminated region and the limited dynamic range of the VNA was not able to capture these subtle changes in the strength of the transmitted signal. It is expected that with reduction in the number of plies and change in their orientations alongside more severe impact conditions inducing carbon fibre fracture, the high frequency SE would be compromised.

5 CONCLUSIONS

Reduced weight with excellent mechanical properties, improved corrosion resistance and design versatility are key drivers in the development of carbon fibre reinforced composites for EMI shielding application as a replacement of commonly used metal alloys. However, as the laminated CFRP structures are particularly vulnerable to impact damage, it is of interest to investigate to what extent the shielding effectiveness is changed for the damaged composites. Electromagnetic shielding durability was investigated in this study for four composite configurations. The panels were first subjected to a low-velocity impact with varying energy and evaluated for the damage size using both pulse-echo ultrasonic scanning and infrared thermography. SE was then measured in the low frequency range using coaxial transmission line method and in the high frequency range using free space technique, where the SE of both pristine and damaged laminates was directly compared. It has been revealed that at low frequencies even barely visible impact damage (BVID) limited to delamination can induce significant changes in the SE frequency response. The SE spectra of the damaged laminates were characterized by multiple ripples with large amplitudes and slightly increased average value. These changes were attributed to the presence of additional interfaces arising from the creation of delaminations between individual carbon fibre plies, which provided additional internal reflections losses inside the composite. The effect was more pronounced for thicker laminates with larger number of delaminated interfaces. On the other hand, no visible changes were observed in the high frequency region, as a result of reduced skin depth and inability of the significant EM wave portion to reach the delaminated region alongside limited dynamic range of VNA measuring strength of the received signal. It is expected that by reducing the number of carbon fibre plies simultaneously to increasing the impact energy to induce carbon fibre damage, the high frequency SE would be compromised. Further study on that aspect should be carried out.

ACKNOWLEDGEMENTS

The authors would like to acknowledge the financial support from the C-Power Ltd and Loughborough University.

REFERENCES

- [1] M. Rudd, T. Baum, B. Mapleback, K. Ghorbani and K. Nicholson, Reducing the attenuation in CFRP waveguide using carbon fiber veil, *IEEE Microwave and Wireless Components Letters*, **71**, 2017, pp. 1089-1091 (doi: [10.1109/LMWC.2017.2762243](https://doi.org/10.1109/LMWC.2017.2762243)).
- [2] N. Dugin, T. Zaboronkova, C. Krafft and G. Belayev, Carbon-based composite microwave antennas, *Electronics*, **9**, 2020, pp. 590-607 (doi: [10.3390/electronics9040590](https://doi.org/10.3390/electronics9040590)).
- [3] G. Artner, R. Langwieser and C. Macklenbrauker, Material induced changes of antenna performance in vehicular applications, *Proceedings of IEEE International Conference on Microwaves, Communications, Antennas and Electronic Systems, Tel-Aviv, Israel, November 2-4, 2015*, pp. 1-4.

- [4] D. Munalli, G. Dymitrakis, D. Chronopolous, S. Greedy and A. Long, Electromagnetic shielding effectiveness of carbon fibre reinforced composites, *Composites Part B*, **173**, 2019, pp. 106906 (doi: [10.1016/j.compositesb.2019.106906](https://doi.org/10.1016/j.compositesb.2019.106906)).
- [5] D. Chung and A. Eddib, Effect of fiber lay-up configuration on the electromagnetic interference shielding effectiveness of continuous carbon fiber polymer-matrix composites, *Carbon*, **141**, 2019, pp. 685-691 (doi: [10.1016/j.carbon.2018.09.081](https://doi.org/10.1016/j.carbon.2018.09.081)).
- [6] X. Luo and D. Chung, Electromagnetic interference shielding using continuous carbon-fibre carbon-matrix and polymer-matrix composites, *Composites Part B*, **30**, 1999, pp. 227-231 (doi: [10.1016/S1359-8368\(98\)00065-1](https://doi.org/10.1016/S1359-8368(98)00065-1)).
- [7] T. Wang, W. Yu, C. Zhou, W. Sun, Y. Zhang, L. Jia, J. Gao, K. Dai, D. Yan and Z. Li, Self-healing and flexible carbon nanotube/polyurethane composite for efficient electromagnetic interference shielding, *Composites Part B*, **193**, 2020, pp. 108015 (doi: [10.1016/j.compositesb.2020.108015](https://doi.org/10.1016/j.compositesb.2020.108015)).
- [8] H. Sim, D. Lee, H. Kim, Y. Jang, G. Spinks, S. Gambhir, D. Officer and S. Kim, Self-healing graphene oxide-based composite for electromagnetic interference shielding, *Carbon*, **68**, 2004, pp. 118-124 (doi: [10.1016/j.carbon.2019.08.073](https://doi.org/10.1016/j.carbon.2019.08.073)).
- [9] S. Schelkunoff, The electromagnetic theory of coaxial transmission lines and cylindrical shields, *Bell System Technical Journal*, **13**, 1934, pp. 532-579 (doi: [10.1002/j.1538-7305.1934.tb00679.x](https://doi.org/10.1002/j.1538-7305.1934.tb00679.x)).
- [10] American Society for Testing and Materials, ASTM Standard test method for measuring the electromagnetic shielding effectiveness of planar materials, American Society for Testing and Materials, 2018.
- [11] Compass Technology Group, CTG-TM-0101-2020 Measuring shielding effectiveness at microwave frequencies with a free-space focused beam, 2020.